

Article

Tribological Properties of Brake Disc Material for a High-Speed Train and the Evolution of Debris

Jinnan Wang^{1,2}, Muhammad Qasim Zafar¹ , Yunbo Chen^{2,3}, Peng Pan³, Lingli Zuo³, Haiyan Zhao^{1,*} and Xiangjun Zhang^{1,*}

¹ State Key Laboratory of Tribology, Department of Mechanical Engineering, Tsinghua University, Beijing 100084, China; wangjinnan@163.com (J.W.); zafarmq10@mails.tsinghua.edu.cn (M.Q.Z.)

² China Academy of Machinery Science and Technology, Beijing 100044, China; cybcamt@126.com

³ Beijing National Innovation Institute of Lightweight Ltd., Beijing 100083, China; ustb_panp@163.com (P.P.); 13811612433@126.com (L.Z.)

* Correspondence: hyzhao@tsinghua.edu.cn (H.Z.); xjzhang@tsinghua.edu.cn (X.Z.)

Abstract: The stability and reliability of braking system are essential factors for the safe operation of high-speed trains. In the proposed work, tribological properties of a newly developed brake disc material namely BD-1 were studied considering the thermal-mechanical effects, as well as the evolutions of wear debris, were particularly examined. The tribological properties were also compared with an existing commercial brake disc material namely BD-2 in text. Friction and wear tests were carried out on BD-1 and BD-2 against a commercial brake pad material (BP) to simulate the real emergence braking conditions of a 350 km/h high-speed railway. The thermal-mechanical coupling effects of the friction velocity, wear mass, temperatures and the friction coefficient were investigated. Local wear track and wear debris were analyzed by using SEM and EDS. Results show that the shape and size of wear debris evolve as the dominant wear mechanism varies during braking tests. As the sliding speed increases from 250 to 1250 rpm, the debris may become fine particles, then into a mixture of lamellar shape and flake shape, and finally becomes fine particles again at high speed. The maximum size of wear debris is first from 20 μm to 65 μm , and then down to 10 μm . As the local area temperature increased by more than 400 °C, debris adhere to the surface forming an adhesive layer that may act as a lubricant. Debris may help to form an adhesive lubrication layer and undertake plastics deformation at the speed range of 500–1000 rpm. The local area temperatures prompted the wear debris adhesion and oxidation. After reaching a certain speed limit, a uniform third body appears to protect the material surface from high speed and high temperature. Results suggested that the BD-1 could be a good candidate braking material for high-speed railway applications.

Keywords: wear mechanisms; brake disc material; coefficient of friction; debris evolution; friction properties



Citation: Wang, J.; Zafar, M.Q.; Chen, Y.; Pan, P.; Zuo, L.; Zhao, H.; Zhang, X. Tribological Properties of Brake Disc Material for a High-Speed Train and the Evolution of Debris. *Lubricants* **2022**, *10*, 168. <https://doi.org/10.3390/lubricants10080168>

Received: 30 June 2022

Accepted: 19 July 2022

Published: 25 July 2022

Publisher's Note: MDPI stays neutral with regard to jurisdictional claims in published maps and institutional affiliations.



Copyright: © 2022 by the authors. Licensee MDPI, Basel, Switzerland. This article is an open access article distributed under the terms and conditions of the Creative Commons Attribution (CC BY) license (<https://creativecommons.org/licenses/by/4.0/>).

1. Introduction

The stability and reliability of braking system are essential factors to guarantee the safe operation of high-speed trains. When trains run at 300 km/h or above they put forward stringent demand on brake disc material that undergo severe service conditions, especially during emergency braking. At present, high-speed train braking mainly depends on disc braking [1,2]. The braking performance directly depends on the local frictional characteristics of the materials interface between the brake disc and brake pad [3]. In a typical braking system of a train, the brake discs adopt cast steel as basic materials, and brake pads are made of copper-based alloy prepared by powder metallurgy [4]. However, material challenges for the brake discs of high-speed trains are still under the spotlight, especially when the train speed is about 300 km/h or more.

First, the temperature rise in the brake disc and brake pad during emergency braking is one of the key challenges in high-speed railways [5,6]. Under braking conditions, local

friction forces on the interface of the brake disc and pad generate a lot of heat, then heat is mainly dissipated by conduction and convection here. Generally, due to differences in thermal capacity and heat conductivity of the disc and the pad materials, most of the friction-induced heat is absorbed by the brake disc itself. Subsequently, the heat will cause physical and chemical reactions on the frictional interface, and then contribute a lot to the development of thermal fatigue and severe wear of the disc and pad [7,8]. Although the thermal fatigue failure mechanism of brake discs has been widely explored so far [9,10] The dynamic contacts between the brake disc and pads inevitably lead to a high friction force accompanied by a huge amount of heat [11–13]. The coupled thermal-mechanical effects not only reduce the braking performance but also lead to the gradual degradation or failure of the brake disc materials.

On another hand, materials of brake disc were not widely reported or studied regarding their tribological characteristics, especially for the braking system of high-speed trains [14–19]. The tribological properties of the potential brake disc materials for high-speed trains are closely coupled with many factors, such as material composition, interface reactions under friction, wear mechanism, as well as wear debris types and evolution process. Kasem et al. [20] used an infrared camera and a two-color pyrometer to monitor temperature evolution during the braking process. The highest temperature of the disc during braking is reportedly close to 900 °C and it was believed that friction and surface wear were closely related to the high temperatures of the friction surface. Ammarullah et al. [21] used finite element model to evaluate the Tresca stress of metal to metal bearings of different metal materials, and explored the influence of stress on wear debris. J. Jamari et al. [22] established A model to study the relationship between contact pressure and wear debris and evaluation of metal-to-metal tribology. Xiao et al. [23] reported that a friction film worked as an intermediate layer and showed a significant effect on protecting the original friction surface materials. Vasiljevic et al. [24] studied the mechanism of particle formation in the brake system. The method of particle measurement in braking process were systematically and comprehensively summarized and discussed, and the study of particle formation mechanism in braking process should be paid attention to in the future. Zhang et al. [25] analyzed the change of the structure and composition of friction film in the wear zone of the brake disc as a result of temperature evolution during braking. Presumably, it was assumed that it is due to the softening of the copper matrix which increases the material transfer rate between friction interfaces. Lyu et al. [26] studied the friction and wear performance of brake discs of different materials at low temperatures, but did not pay attention to the debris generated in the friction process. Wang et al. [27] analyzed the influence of brake disc crack propagation and microstructure evolution on the formation of a white etching layer on the surface, however, the effect of running speed on wear debris was overlooked. Riva et al. [28] performed an experimental investigation where wear debris were obtained from pin-disc tribometer tests, but the mechanism and composition of debris were not covered in the investigation. Rodrigues et al. [29] studied the lubrication effects of CuO, Fe₂O₃ and Fe₃O₄ mixture at different temperatures by adding the mixture of CuO, Fe₂O₃ and Fe₃O₄, and graphite particles into the local area of a pin-disc friction test, and the results showed that the friction coefficient of CuO, Fe₂O₃ and Fe₃O₄ mixture was low when tested at 400 °C, which suggested that the particle mixture may play a lubricant role at high temperature. However, the resulted wear debris during the friction process were not collected and analyzed.

In this paper, a newly developed alloy was adopted as brake disc material and compared with a commercial brake disc material considering their friction and wear mechanisms by forming dry frictional pairs against copper-based powder metallurgy material as brake pad. This article adopts the emergency braking pressure as the test pressure to reveal the real working conditions. The brake discs and pads undergoing different thermal-mechanical conditions were investigated. Relationships between friction coefficient, wear topography, wear surface metallography, evolution of wear debris type, and composition elements were particularly examined and analyzed.

2. Materials and Methods

A newly developed brake disc material is adopted and termed BD-1 alloy. The alloy was smelted by a vacuum induction furnace. Then it was normalized, hardened, and tempered before being made into specimens. The normalizing temperature was 950 °C and the quenching temperature was 920 °C. The tempering temperature was 600 °C. Finally, the brake disc specimens of BD-1 material were obtained. A commercial brake disc material (named BD-2) which serves for the 300 km/h speed class was also chosen for comparison. The composition of the BD-1 and BD-2 brake discs were shown in Table 1.

Table 1. Material compositions of brake discs (BD-1, BD-2) (wt%).

Element	C	Si	Cr	Mo	Ni	Mn	V	Fe
BD-1	0.30	0.50	1.60	0.8	0.95	1.0	0.1	Bal.
BD-2	0.22	0.41	0.80	1.0	0.95	1.0	-	Bal.

Copper-based brake pads were adopted as a counterpart in the tests due to their high thermal conductivity and the ability to stabilize the coefficient of friction under critical service conditions [30,31]. The copper-based brake pads were taken from a commercial brake pad (named BP). The composition is shown in Table 2. The surface roughness of the specimen Ra is 0.8 μm. Vickers hardness tester (FE800, Future-tech, Kanagawa, Japan) was used to measure the microhardness of materials.

Table 2. Material compositions of brake discs (BP) (wt%).

Element	Cr	S	C	Mo	Fe	Cu
BP	6.5	1.6	12.4	2.1	16.6	Bal.

The friction test samples and the contact configuration are shown in Figure 1a. The tribological tests were performed using unidirectional sliding motion on a pin-on-disk tribometer (MMU-10G, Nuo Century Test Instrument Co. Ltd., Jinan, China) following ASTM G99 standard. The upper pin specimen was made of brake disc material BD-1 or BD-2. The bottom specimen was made of brake pad material BP. The normal load was kept as constant as 120 N, which results in an average contact pressure of 1.60 MPa. To simulate the real working conditions of thermo-mechanical effects, the rotating speeds were selected as 250 rpm, 500 rpm, 750 rpm, 1000 rpm, and 1250 rpm separately. With a rotating diameter of 21.0 mm. The resulted velocities were 0.275 m/s, 0.55 m/s, 0.825 m/s, 1.1 m/s, 1.375 m/s. A thermocouple was bonded close to the sliding track to record the temperature rise during the frictional test, as shown in Figure 1b. The dry sliding tribological tests were carried out at ambient room temperature and humidity. The specimens were put into anhydrous ethanol for ultrasonic cleaning for 5 min and finally dried with a hot air blower before the test. For every test, the running-in time was selected as 10 min, then the originally resulting wear debris was blown out by a gas blower to begin a normal friction test.

The normal friction test time of each group was kept as 30 min. Each experiment was repeated three times and the wear debris were collected after each test. High-precision electronic balance was used to weigh the samples. Different techniques have been used to observe and characterize the friction interface and wear debris, such as optical microscope (BX51M, Olympus, Tokyo, Japan), white light interferometer (NeXView, ZYGO, Middlefield, CT, USA), SEM (Gemini-300, Zeiss, Oberkochen, Germany), and EDS analysis. The SEM (Gemini-300, Zeiss, Oberkochen, Germany) and EDS (Ultim, Oxford, UK) are used to observe the surface structure of the wear surface and analyze the types and contents of elements in the wear surface.

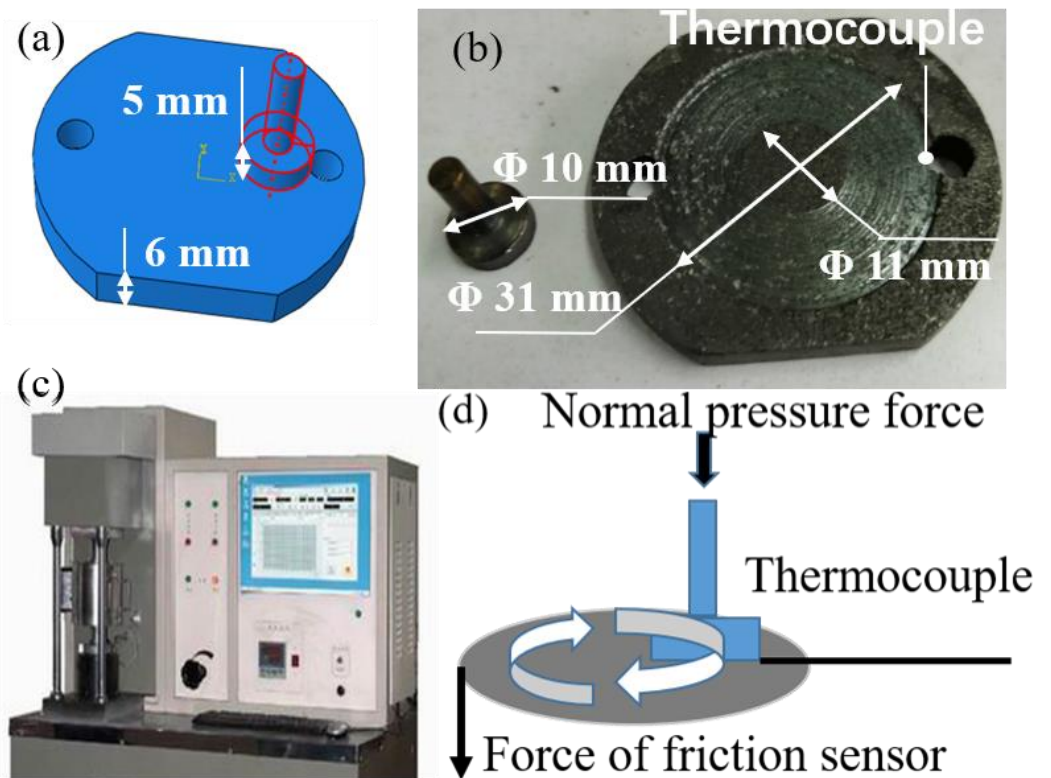


Figure 1. The contact figures of samples: (a) Contact figures of the pin-on-disc pair. The pin is made of material BD-1 or BD-2, and the disc is made of material BP; (b) Sample sizes for the frictional test. (c) Equipment detail; (d) Schematic diagram of the test device.

3. Experimental Results

3.1. Friction Coefficient and Fluctuations

Figure 2 shows typical evolution curves of coefficient of friction (COF) for the conditions under-selected rotational speeds in experimental trial. The variations of COF for both BP-1 and BP-2 materials are illustrated in a series Figure 2a–j. The COF of BD-1 presents a similar fluctuation trend as that of BD-2 at various tested velocities. The COFs present a sharp increase in the start period and gradually stabilize over time. Generally, the COFs first increase with the sliding speed, reaches a maximum value, then gradually decrease, and finally tend to be constant. After a beginning frictional time, the friction coefficients reach a stable value and then decrease and flatten. This beginning is longer or shorter depending upon the friction properties of the materials. This indicates that the interface evolution may play a role in the variations of the COF.

The mean COF is obtained by removing the run-in period data from the collected data. The fluctuation range of average COF for the two materials is also shown in Table 3. The mean COFs of BD-1 and BD-2 presents near the same value except those at 1000 rpm.

Table 3. COF fluctuation amplitude and mean COF.

NO	Mean COF for BD-1	COF Fluctuation Amplitude of BD-1	Mean COF for BD-2	COF Fluctuation Amplitude of BD-2
250 rpm	0.73	0.45–0.50	0.72	0.48–0.68
500 rpm	0.57	0.21–0.32	0.56	0.32–0.52
750 rpm	0.5	0.13–0.28	0.55	0.28–0.43
1000 rpm	0.54	0.22–0.32	0.39	0.30–0.48
1250 rpm	0.60	0.32–0.68	0.59	0.40–0.78

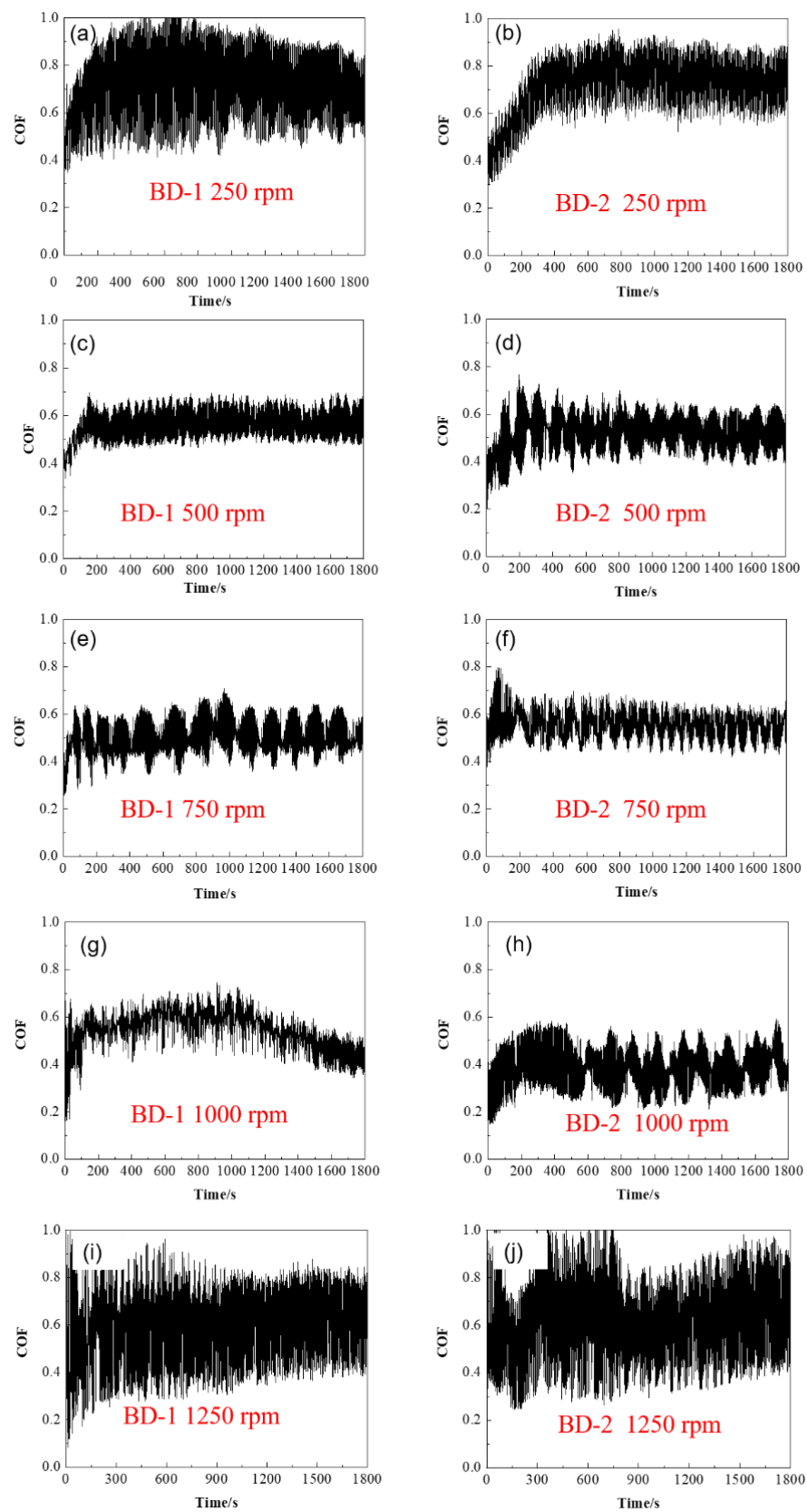


Figure 2. Variation of COFs for BD-1 and BD-2 at designed rotational speeds: (a) BD-1 at 250 rpm; (b) BD-2 at 250 rpm; (c) BD-1 at 500 rpm; (d) BD-2 at 500 rpm; (e) BD-1 at 750 rpm; (f) BD-2 at 750 rpm; (g) BD-1 at 1000 rpm; (h) BD-2 at 1000 rpm; (i) BD-1 at 1250 rpm; (j) BD-2 at 1250 rpm.

To compare the friction performance of BD-1 and BD-2, the COFs and fluctuation bars are presented in Figure 3. The corresponding near-local area temperatures are also presented according to the preset thermocouple, as blue line and pink line indicated in Figure 3. It can be seen that the near-local area temperature increases with the velocity. The COFs of BD-1 and BD-2 are similar at various speeds, except for the minor difference at 750 rpm and significant difference at 1000 rpm. The COFs fluctuation of BD-1 was smaller than that of BD-2 except for the speed of 1000 rpm.

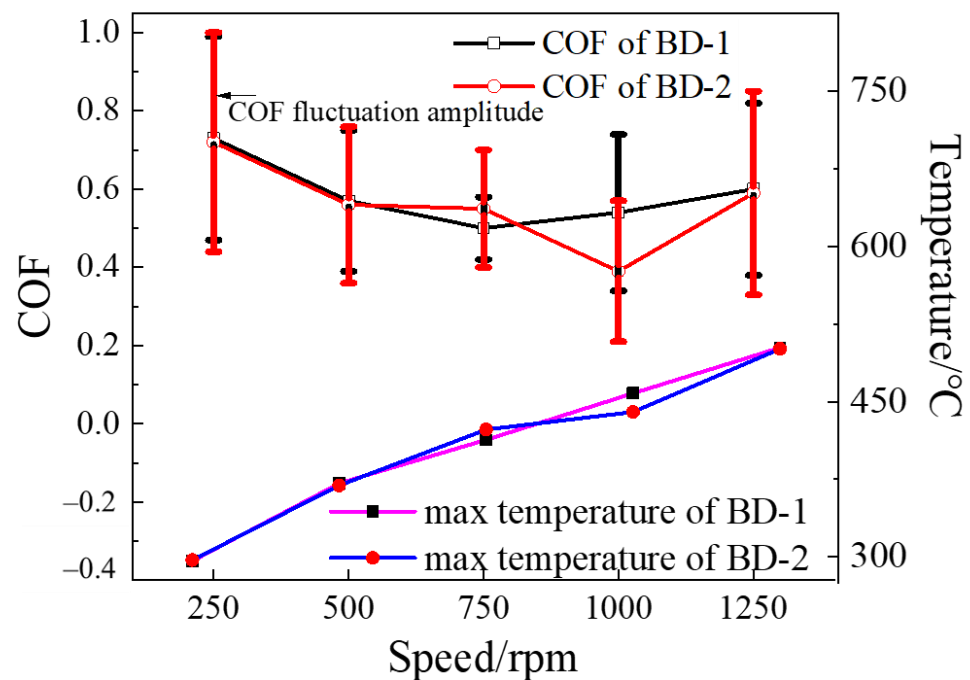


Figure 3. Mean COFs, COF fluctuations and local area max temperatures of frictional pairs at different rotating speeds.

The COFs differences and fluctuations also reflect on the temperature differences, since the friction coefficient may cause the change of frictional heat and then affect the temperature directly. The frictional temperature may change the interface properties of the materials so that the friction coefficient and the fluctuations may vary a lot vice-versa. The difference of COFs of frictional pairs corresponds to the difference of local area temperatures quite well from Figure 3.

However, the fluctuation range of COF varies greatly under different rotational speeds as illustrated in Figure 2a–j. The amplitude of COF present significant fluctuations at low speeds (250 rpm), as well as at high speed (1250 rpm). As the local area temperatures were quite different, i.e., 296 °C at 250 rpm and upto 502 °C at 1250 rpm, the COF fluctuations may indicate a role of the contact interface evolutions and the coupling interaction of the interfacial heat. Thus the thermal-mechanical effects may attribute to the COF fluctuation here.

Furthermore, the wear mass loss of BD-1 and BD-2 at different speeds were measured and presented in Figure 4. It can be observed that the wear mass loss of the two materials is quite different. The wear mass loss of BD-1 decreases first with the rotation speed, then it goes up to a maximum value at 1000 rpm and then goes down at 1250 rpm. The wear mass loss of BD-2 first increases with the rotation speed until 750 rpm and then decreases from speed of 1000 rpm and reaches a minimum value at 1250 rpm. This shows that BD-2 begin to present a higher wear at 750 rpm, which is more sensitive to speed than BD-1.

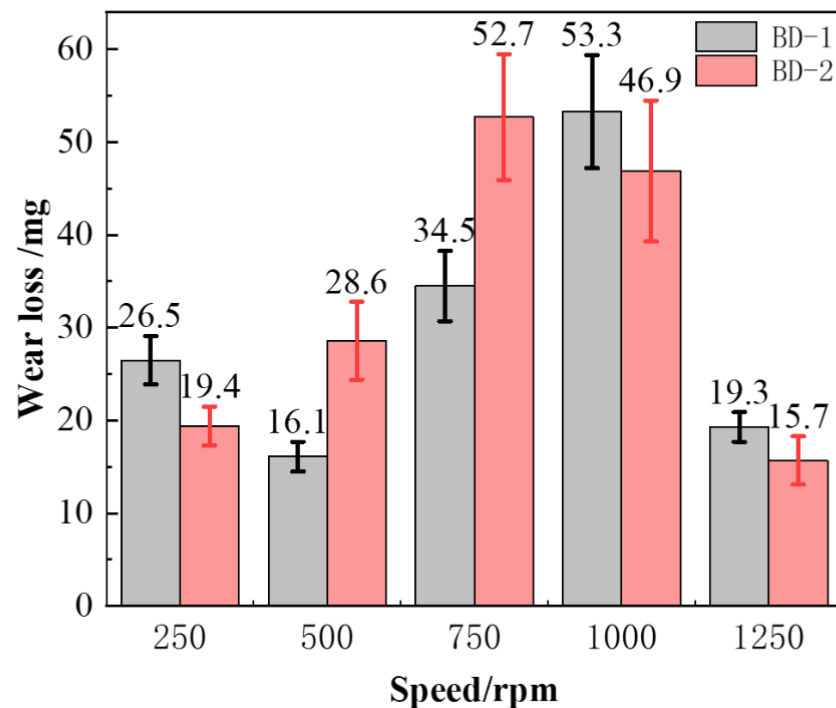


Figure 4. Wear mass loss of BD-1 and BD-2 at different rotational speeds.

The wear mass of BD-2 is 75.1% higher than that of BD-1 at 500 rpm, 53.3% higher than that of BD-1 at 750 rpm. Thus the newly developed BD-1 material presents a better anti-wear performance compared with the commercial material BD-2.

3.2. Wear Surface Observation

The surface topography of wear tracks was observed by SEM as shown in Figure 5. The corresponding speeds are also labeled, the left column indicates the surface topography of BD-1 and the right column is that of BD-2. They all present wear scratches along the sliding directions, which indicates the wear tracks. After the cleaning process before SEM observations, the observed dark area on the wear tracks indicates an adhesive layer of debris or interface reaction layers occurred during the friction process. Generally, the wear track surfaces of BD-1 are clear and dominated by obvious mechanical scratches, except those dark area at speeds of 750 rpm and 1000 rpm. In contrast the wear track surfaces of BD-2 present deeper scratches, and begin to have adhesion-like dark area at 500 rpm, 750 rpm, and 1000 rpm. It should be mentioned that the 5 images with adhesion-like areas are connected with highest wear rates in Figure 4.

Both the worn surfaces were characterized by mechanical wear accompanied by subtle adhesive wear as shown in Figure 5a–d represent friction surface at 500 rpm and it can be seen that wear tracks become shallow in BD-1 and relatively severe adhesive wear in BD-2. The analysis suggested that the deep scratches in BD-2 could be associated with low hardness of corresponding material. Since the hardness of BD-1 and BD-2 is 435 HV0.2 and 360 HV0.2, respectively. Therefore, the wear scratch depth is closely related to the hardness of the material.

From Figure 5e,f at speeds of 750 rpm, BD-1 and BD-2 present similar dark adhesive layer distribution on the surfaces. Note that indicates in Figure 2e,f, both the two materials have a similar COF curve as at 750 rpm. Since both the COF curves present minor fluctuation, this suggests that the wear mechanism involves here may related to a combination of mechanical scratch wear and adhesive wear.

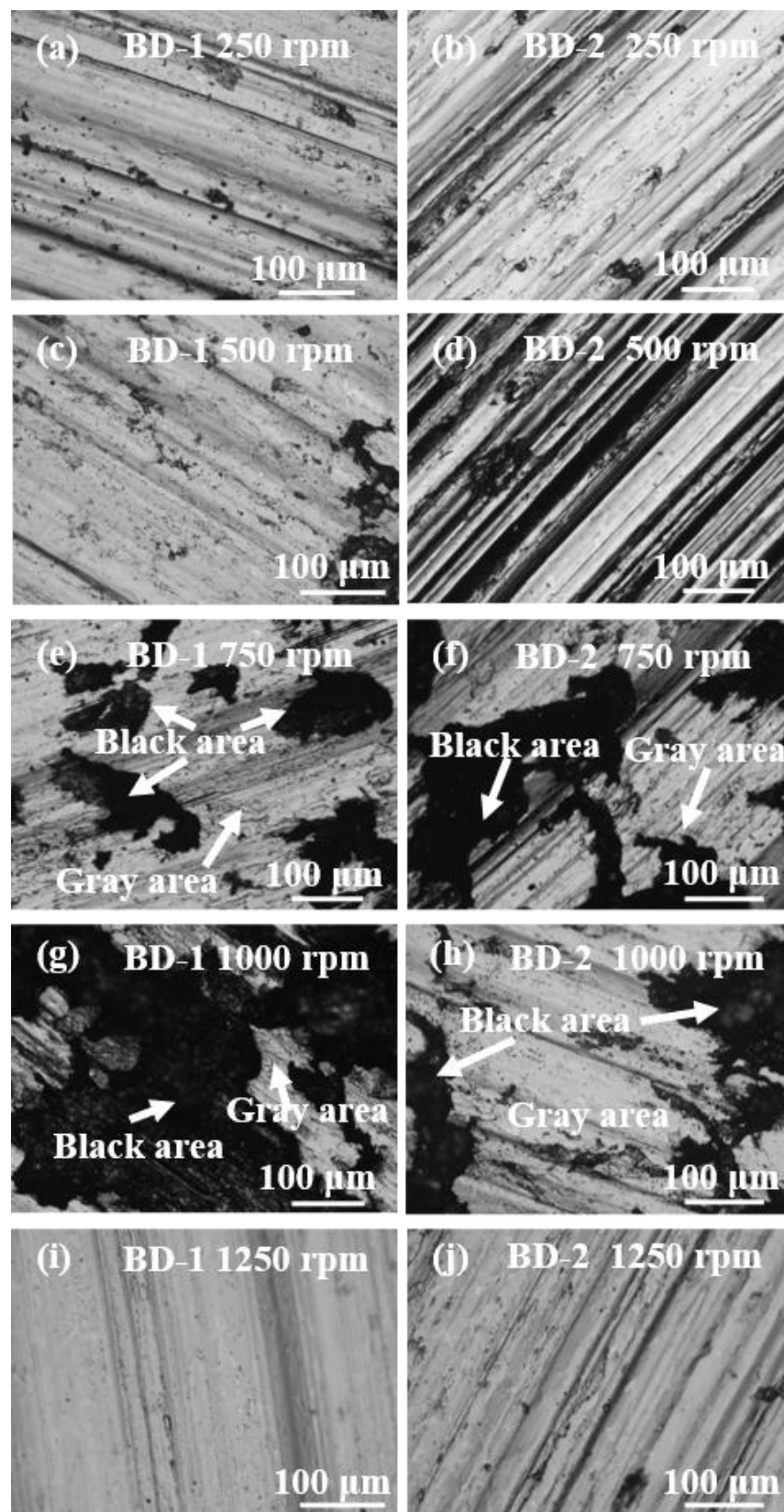


Figure 5. Surface morphology of BD-1 and BD-2: (a) BD-1 at 250 rpm; (b) BD-2 at 250 rpm; (c) BD-1 at 500 rpm; (d) BD-2 at 500 rpm; (e) BD-1 at 750 rpm; (f) BD-2 at 750 rpm; (g) BD-1 at 1000 rpm; (h) BD-2 at 1000 rpm; (i) BD-1 at 1250 rpm; (j) BD-2 at 1250 rpm.

As illustrated in Figure 2g,h for 1000 rpm, BD-1 presents more stable COFs compared to BD-2. Correspondingly, it is obvious that BD-1 has a larger area and more uniform black adhesive layer on wear track in Figure 5g compared with that of BD-2 in Figure 5h. This may further suggest that the adhesive layer may play a key role in frictional behavior as speed increases upto 1000 rpm. Relating the wear mass loss results in Figure 4, it can be seen that speed of 1000 rpm is the maximum and turning point of wear loss quantity for BD-1. The surface morphology of BD-1 at 1000 rpm is fully covered by the adhesive layer, which indicates that the adhesive layer is closely related to wear mass loss, thus allied with wear debris. Meanwhile, the maximum and turning point of wear loss quantity for BD-2 occurs at speed of 750 rpm, corresponding to its wear track being largely covered by the adhesive layer.

However, as the sliding speed increase further upto 1250 rpm, the dark adhesive layer disappears both on BD-1 and BD-2. The wear surface on BD-1 becomes smoother than that of BD-2.

To explore the evolution process of the adhesive layer, the energy spectrum of the local wear track surface at 1000 rpm was tested and studied, as shown in Figure 6.

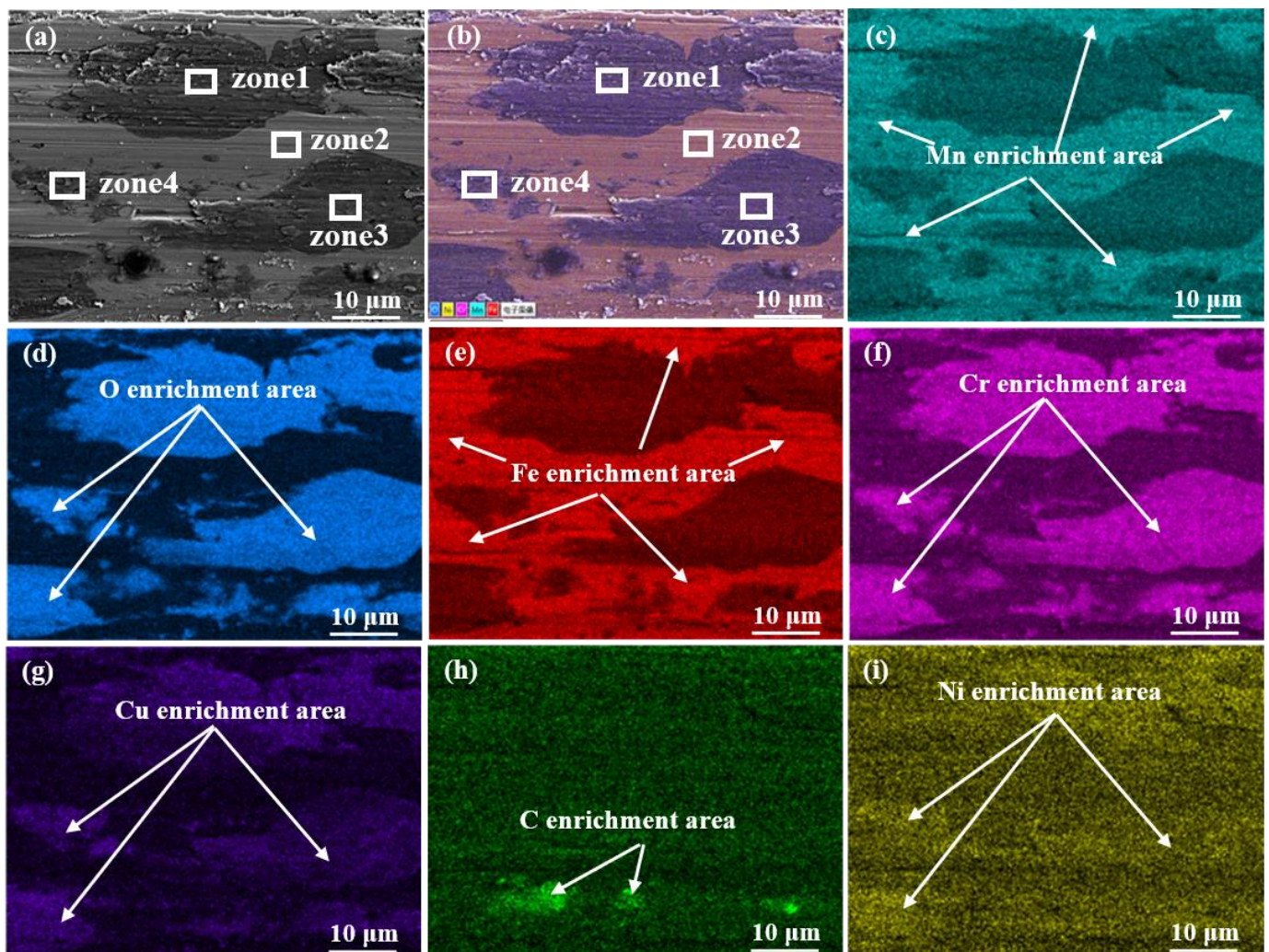


Figure 6. SEM and energy spectrum images of wear surface of BD-1 after testing at 1000 rpm: (a) SEM image; (b) Comprehensive energy spectrum image; (c) Energy spectrum of Mn; (d) Energy spectrum of O; (e) Energy spectrum of Fe; (f) Energy spectrum of Cr; (g) Energy spectrum of Cu; (h) Energy spectrum of C; (i) Energy spectrum of Ni.

First, the wear track area can be divided into different regions, as seen in Figure 6a,b. Zone 1 indicates the largest dark area, zone 2 shows light-color region, zone 3 is termed for another dark region, and zone 4 is the transition region. It displays from Figure 6c,e that manganese and iron element are enriched in the light-colored region of zone 2. Compared with the light-color area, oxygen element, chromium element, and copper element are enriched in the dark area according to Figure 6d–g. Distribution of carbon elements and nickel elements in the two regions is given in Figure 6h,i without much difference.

The element composition of the four regions is listed in Table 4.

Table 4. Composition of the four regions in Figure 6a. (at%).

NO	Fe	C	Mn	Cr	Ni	Si	Mo	V	O	Cu
Total	53.2	8.7	0.6	5.1	0.0	0.6	0.2	0.0	29.1	2.5
Zone1	38.3	6.7	0.0	7.8	0.0	0.6	0.2	0.0	44.3	2.2
Zone2	77.2	10.1	2.5	5.8	0.8	0.7	0.2	0.0	2.7	0.1
Zone3	35.5	6.9	0.0	5.0	0.0	0.4	0.2	0.0	47.8	4.3
Zone4	38.3	6.5	0.0	7.7	0.0	0.5	0.2	0.0	44.1	2.7

From Table 4, the element content of zone 2 includes a highest Fe of 77.2 a%, a lowest oxygen of 2.7%, medium chromium of 5.8% among the four regions. The content is consistent with that of BD-1 base materials, indicating that zone 2 is close to the original substrate materials. Zone 2 maybe labeled as substrate area. Zone 3 has the lowest Fe element of 35.5%, a highest Cu element of 4.3% among the four regions, and the highest oxygen of 47.8%. Chromium is higher than that in zone 2. These suggest that zone 3 interacts strongly with the counterpart (i.e., the BP materials), and copper oxide and iron oxide exist more in zone 3. Zone 3 maybe labeled as oxidized area. For zone 1 and 4, the oxygen content is slightly lower than that of zone 3, which is 44.3% and 44.1%, respectively. Copper is 2.1% and 2.7%, and chromium is 7.8% and 7.7%, respectively. The results may suggest that there is higher chromium in the transition zone between the oxidized zone 3 and the substrate zone 2. It is clear that the ‘dark zones’ are composed by oxides of Cr (and some Cu).

Furthermore, the BD-1 material tested after 1250 rpm was analyzed by SEM, as shown in Figure 7. It can be seen from Figure 7a,b that there is a uniform film on the wear track after a test of 1250 rpm. Its elemental composition (as in Table 5) is rich in CuO, Fe₂O₃ and Fe₃O₄, but is different from BD-1 substrate materials or the counterpart BP materials. This suggests that the high temperature on the contact area may promote the formation of a layer of third body film, which may be resulted from the thermal-mechanical coupling effects on the frictional local area at high speed. This layer may come from the uniformly adhered dark layer (as indicated in Figure 5g), become oxidized further due to the thermal-mechanical effects, and finally provide a protection for the friction pair materials to shallow the wear scratches (as indicated in Figure 5i) and meanwhile reduce the wear mass loss (as in Figure 4). Thus the evolution of the interface layer during the friction process play a key role to protect the material surfaces.

Table 5. Composition of total area in Figure 7a. (at%).

NO	Fe	C	Mn	Cr	Ni	Si	Mo	V	O	Cu
Total	20.2	9.5	0.0	2.4	0.0	0.4	0.2	0.0	39.9	27.4

3.3. Wear Debris Evolution

Many particles accumulate around the local area in the process of friction and wear test. The total number, size, chemical composition and morphology of particles closely interact with the wear mechanism evolution. Thus the grinding debris produced in the experiments were collected and then observed by SEM. Results are shown in Figure 8. The left column is the debris of BD-1 and the right column comes from the debris of BD-2.

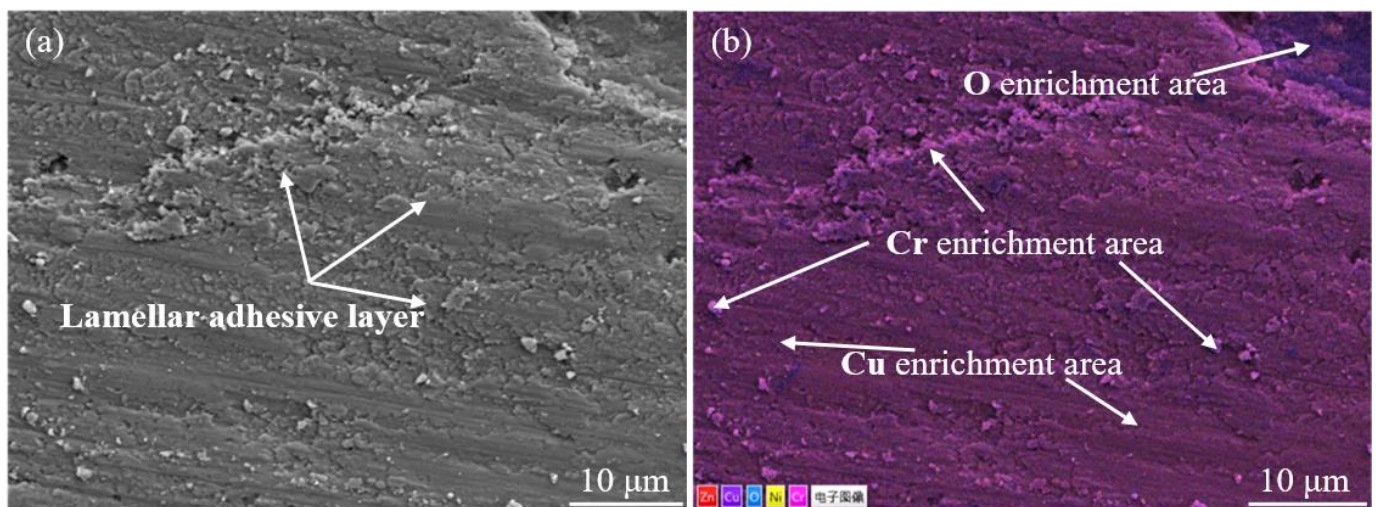


Figure 7. SEM and energy spectrum images of wear surface after testing at 1250 rpm of BD-1 material. (a) SEM images; (b) EDS image.

For BD-1 material in the left column, the debris size is small at speed of 250 rpm, then increases with the increase of sliding speed. The shapes transform from minor particles at 250 rpm to lamellar at 750 rpm, then to big blocks at 1000 rpm, and finally become fine particles again at 1250 rpm. At speeds of 750 rpm and 1000 rpm, particles appear as a mixture of lamellar and granular phases with a maximum size above 20 μm . While in the right column BD-2 presents a mixture phase of large block and lamellar debris from the beginning of speed 250 rpm, the sizes of lamellar debris increase with the speed obviously, until the debris becomes fine particles at 1250 rpm. The lamellar debris size of BD-2 increased from 45.6 μm to 80.1 μm when the rotation speed increases from 750 rpm to 1000 rpm. Wei li et al. [32] research suggests that in the process of contact sliding, debris plays an important role in the surface wear and damage evolution of corresponding materials, and desize of debris affects the mechanism of surface damage evolution.

Generally, BD-2 presents a larger debris size compared with BD-1. After the test of 500 rpm, the maximum abrasive size of BD-1 and BD-2 was 16 μm and 30 μm , respectively, and the particle shape was flat block. Similarly, after the 750 rpm test, the maximum particle size of BD-1 is about 30 μm , and the maximum particle diameter of BD-2 is 50 μm . Moreover, at 1000 rpm, the maximum particle size of BD-1 is about 50 μm with square block morphology, while the maximum particle size of BD-2 is 65 μm in lamellar shape. Finally, the abrasive particles of the two materials are less than 10 μm and relatively fine and uniform after a test of 1250 rpm. Especially, the differences in debris size and shape of BD-1 and BD-2 at speeds of 500 rpm and 750 rpm correspond quite well with the differences in mass loss of BD-1 and BD-2 shown in Figure 4. These suggest that BD-1 material has a smaller debris and lower wear loss compared with BD-2, which could be a better candidate material for high-speed brake discs.

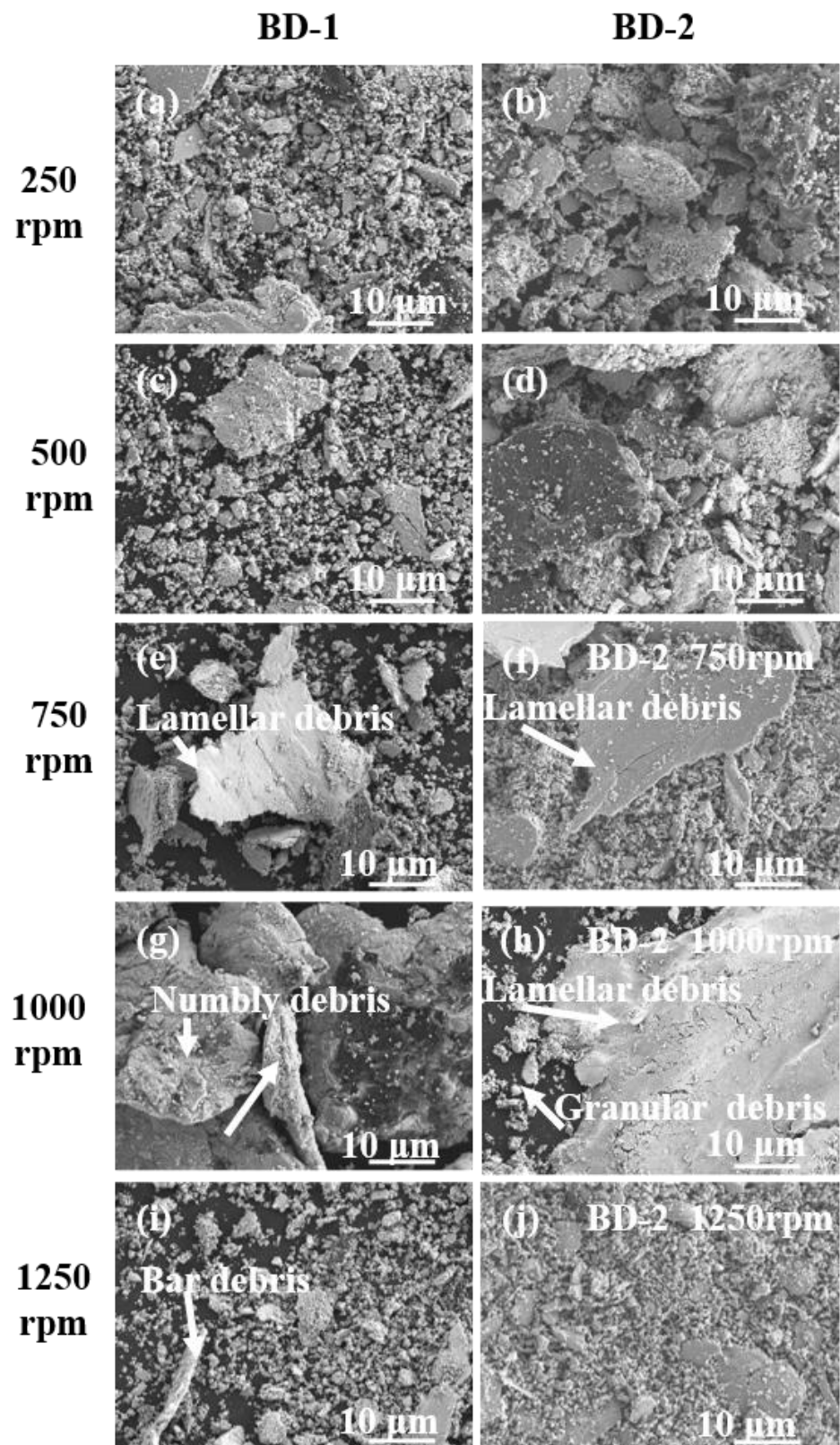


Figure 8. Debris morphology of BD-1 and BD-2 after different test conditions. (a) BD-1 at 250 rpm; (b) BD-2 at 250 rpm; (c) BD-1 at 500 rpm; (d) BD-2 at 500 rpm; (e) BD-1 at 750 rpm; (f) BD-2 at 750 rpm; (g) BD-1 at 1000 rpm; (h) BD-2 at 1000 rpm; (i) BD-1 at 1250 rpm; (j) BD-2 at 1250 rpm.

4. Discussion

The COF of both BD-1 and BD-2 present similar curves against sliding speed. The friction coefficient of the friction layer containing ferromagnetic iron oxide is usually reported between 0.48 and 0.55 [33,34]. The COFs of both materials quickly rise from the initial 0.35 to the maximum value of 0.9 and then became stable as shown in Figure 2. The average COF in the friction test is 0.5–0.8 with 0.30 approximate variation amplitude. Generally, average COF decreased with the increase in rotational speed. The fluctuation of friction coefficient becomes significant at a low speed of 250 rpm and a high speed of 1250 rpm.

Since the test load is relatively large to simulate the emergency braking process, the variations in speed will result in obvious local temperature variations for the friction pairs. Thus the whole tribological behaviors are dominated by a thermal-mechanical coupling process, including the COF fluctuations, local oxidation layer, debris, and third body film.

The evolution of wear debris and COF with the thermal-mechanical coupling process (i.e., temperature and speed at a constant pressure in this study) is summarized in Figure 9. As the rotational speed increases, the temperature of the friction contact surface increases, both of which are labeled on the x axis. With the increase of rotational speed, the friction coefficient decreases first and then increase as the top two lines indicate, meanwhile the debris size increases first and then decreases as the bottom curves indicates.

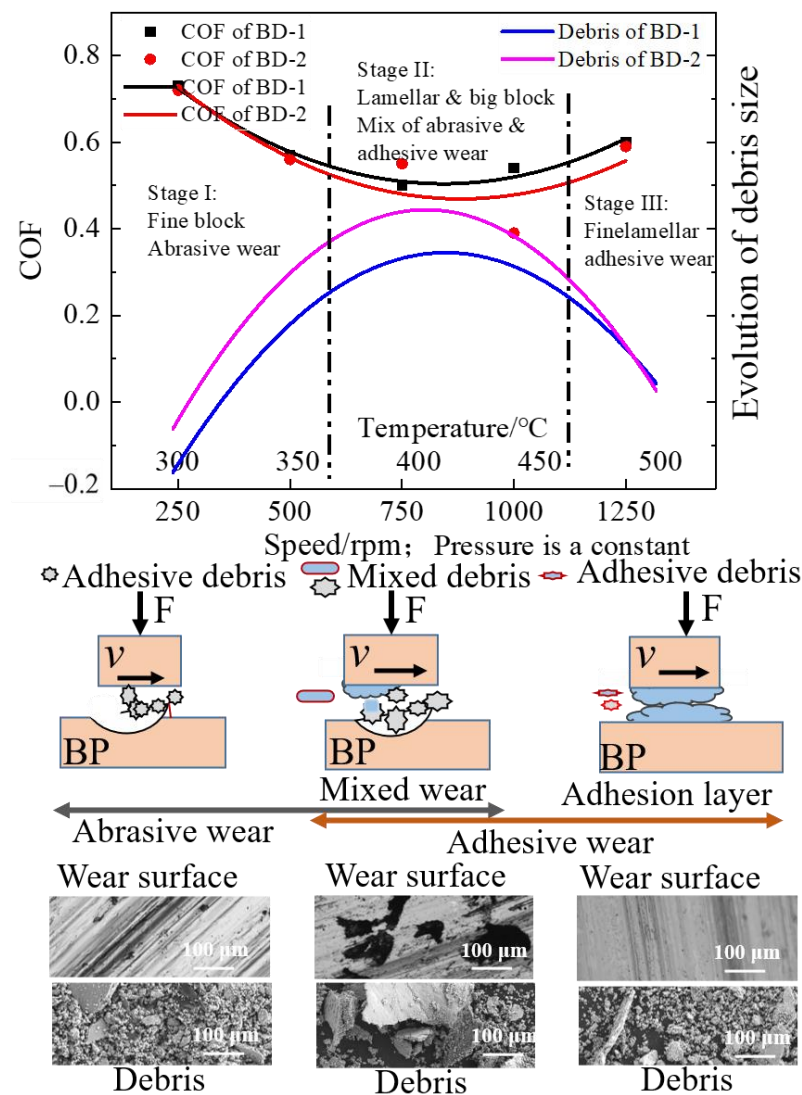


Figure 9. Evolution of debris and adhesion layer formed on the interfaces.

In Figure 9, the wear mechanism and the evolution of debris are divided into three stages, as the vertical dash lines indicate. Referring to Figure 8, we can see that in stage I, debris presents a small fine particle shape, indicating a mainly abrasive wear mechanism. In stage II, debris present a mixture phase of lamellar particles and big blocks, the wear mechanism becomes both abrasive wear and adhesive wear together. In stage III as the speed increase further, wear debris becomes fine lamellar particle again, but the wear mechanism becomes adhesive wear dominated since a third body layer is observed to be formed on the interface as Figure 7 indicates.

Debris may play a key role in COFs fluctuation. First, at a low speed of 250 rpm, the frictional pairs may form a close contact. The friction coefficient fluctuates greatly due to the original roughness of the sample surface, and the resulted fine debris also cause the fluctuation of COF here. However, due to the relatively lower temperature at this stage, it is not easy for the debris to form an adhesive layer. As the local temperature rises with the sliding velocity, local temperature causes more and more debris to adhere to the interface, forming an oxidation layer and playing a lubrication role on the COFs. Thus the COFs fluctuation decreased in stage II. However, the wear loss increases significantly at this speed range, since the friction force causes a repeatable removal of the damaged adhesive layer and continuous formation of a new adhesive layer. At speed of 1250 rpm, the local temperature was above 502 °C, the high temperature cause a third body uniform layer on the contact surface, which may prevent the adhesive layer from removing. The close contact between the contact surfaces may also result in a higher COF fluctuations. However, the resulted debris becomes fine and small in size again. Thus the whole wear loss decreases significantly as shown in Figure 4. Of course, the point temperature of 502 °C does not directly indicate the temperature of the local contact area, which may be even higher to form a third body adhesive layer.

Debris characters are dependent on the sliding velocity and the local temperatures, thus resulting in different wear losses. First, the friction velocity affects the shear strain by affecting the contact time of the contact surface [34–37]. From low to high speed, the contact time of the friction pair will decrease and subsequently; COF will reduce as the shear strain of the local contact materials decrease. Another hand as the speed increase, the dry friction coefficient evolves into two stages: interface matching and plastic deformation [38]. At low speed, mechanical wear from the interface matching contact dominates, the wear debris is fine particles, as shown in Figure 8a. It indicates a typical abrasive wear. As speed increases, higher local temperature drives debris to be adhered to the interface and involved into the plastic deformation in the local area, as well as the oxidation reaction that occurs in the contact area. Thus the debris may transfer into an adhesive layer (dark area in Figure 5) and play a significant role in lubrication. This resulted debris presenting a mixture of lamellar shape and flake shape (as shown in Figure 8c–f). They are essentially produced by continuous plastic deformation and oxidation, indicating that the plastic deformation of the contact area dominates here. Thus wear mechanism changes into adhesive wear gradually with the increase of rotational speed. When the local temperature increase further until a uniform third body film is formed, the new closely matched interface appears, COFs begin to fluctuate largely but the average COFs decrease (refer to Figure 3), debris become into fine particles again (refer to Figure 8) and the wear loss decrease significantly (refer to Figure 4). This third body layer will protect the sliding surfaces at high speed and high temperatures.

The two kinds of braking materials are compared according to the tribology properties and debris evolutions. Perhaps, BD-1 and BD-2 present similar COF curves. The main COF differences occur between the rotation speed 750 rpm–1000 rpm. The differences in wear mass loss occur between the rotation speed 500 rpm–750 rpm. BD-1 presents a significantly less wear loss than BD-2. SEM analysis of the local surface also show that the adhesive layer presents a better lubrication role on BD-1 and the depth of wear scratch on BD-1 is shallower than BD-2. Debris observation also reveals that the debris size and shape of BD-1

are better than that of BD-2. Therefore, BD-1 is suggested to be a better candidate braking material for high-speed railway applications.

5. Conclusions

A newly developed material BD-1 was trialed to embrace as brake disc material in high-speed trains and was compared with existing commercial brake disc material BD-2 in terms of COF, wear mass loss, surface SEM observations, and debris analysis. Their tribological properties are affected by coupling functions of rotation speed, local temperature, local area reaction, debris characters and deformation mechanism. Current experimental studies have certain limitations in throwing with actual service in high speed and extreme service environments.

Average COF of BD-1 and BD-2 decreased with the increase of rotational speed. Fluctuations in the coefficient of friction interact with local temperatures and the characters of debris. Debris characters evolve as the speed increases. Debris may help to form an adhesive lubrication layer and undertake plastics deformation at the speed range of 500 rpm–1000 rpm. The local area temperatures prompt the wear debris adhesion and oxidation, and the wear mechanism of brake materials transfer from abrasive wear to adhesive wear, until a third body film formed on the contact area under high temperature owing to high speed of the train. The third body film results in a lower COF, lower wear mass loss, finer debris size, and protects the material surface from high speed and high temperature. BD-1 material demonstrated a similar COF curve as a commercial material BD-2, but it has significantly less wear loss, finer debris size and shape, and can form a uniform adhesive layer at high temperature, thus is suggested to be a better candidate braking material for high-speed railway applications. The research also provides an approach to evaluate the brake disc materials and reveal their friction and wear mechanism. In order to be more consistent with the actual environmental temperature changes, we will study the friction and wear mechanism in various service environments in the future.

Author Contributions: J.W.; conceptualization, methodology, experimentation, writing and editing. M.Q.Z.; methodology, writing, editing, proofreading, Y.C.; conceptualization, funding. L.Z.; validation data curation. P.P.; validation, H.Z.; conceptualization, supervision, review, funding. X.Z.; supervision, conceptualization, guidance, review and editing, funding. All authors have read and agreed to the published version of the manuscript.

Funding: This work was funded by the National Natural Science Foundation of China (Grant No. 51975320), the Beijing Natural Science Foundation (No. M22011), and the National Key R&D Program of China (No. 2017YFB1103300).

Institutional Review Board Statement: Not applicable.

Informed Consent Statement: Not applicable.

Data Availability Statement: Experimental data would be available on request.

Acknowledgments: We want to extend our gratitude to Tongwei Shao for his contribution to the experimentation trial.

Conflicts of Interest: The authors have no competing interests to declare that are relevant to the content of this article.

Nomenclature

Nomenclature of physical quantities and abbreviations appear in this paper.

SEM Scanning Electron Microscope

EDS Energy Dispersive Spectroscopy

COF Coefficient Of Friction

BD-1 A newly design brake disc material; Alloy powder purchased from Trillion Metals Co.,Ltd.

BD-2	A commercial brake disc material (Knorr, CRCC TKD-DS64)
BP	Copper-based brake pad of commercial materia (Knorr, CRCC UPE-DP18)
C	Carbon element
O	Oxygen element
Fe	Ferrum element
Si	Silicon element
Cr	Chromium element
Mn	Manganese element
V	Vanadium element
Fe ₃ O ₄	ferroferric oxide
Ni	Nickel element
Mo	Molybdenum element
Cu	Cuprum element
F	force Unit N. The force of experiment.
<i>v</i>	Linear velocities in the experiment
Fe ₂ O ₃	ferroferric oxide
CuO	Copper oxide

References

- Xiao, J.-K.; Xiao, S.-X.; Chen, J.; Zhang, C. Wear mechanism of Cu-based brake pad for high-speed train braking at speed of 380 km/h. *Tribol. Int.* **2020**, *150*, 106357. [[CrossRef](#)]
- Mann, R.; Magnier, V.; Brunel, J.F.; Dufrénoy, P.; Henrion, M.; Guillet-Revot, E. Thermomechanical characterization of high-speed train braking materials to improve models: Numerical validation via a comparison with an experimental braking test. *Tribol. Int.* **2021**, *156*, 106818. [[CrossRef](#)]
- Vorobyev, A.A.; Kulik, V.I.; Nilov, A.S.; Spiriyugova, M.A. Promising technologies for the production of brake discs from SiC ceramic matrix composites for braking systems of high-speed railway transport. *Proc. Petersburg Transp. Univ.* **2020**, *3*, 378–386. [[CrossRef](#)]
- Niu, J.; Wang, Y.; Wu, D.; Liu, F. Comparison of different configurations of aerodynamic braking plate on the flow around a high-speed train. *Eng. Appl. Comput. Fluid Mech.* **2020**, *14*, 655–668. [[CrossRef](#)]
- Zhang, P.; Zhang, L.; Fu, K.; Wu, P.; Cao, J.; Shijia, C.; Qu, X. Effects of Ni-Coated Graphite Flake on Braking Behavior of Cu-Based Brake Pads Applied in High-Speed Railway Trains. *J. Tribol.* **2019**, *141*, 081301. [[CrossRef](#)]
- Tavangar, R.; Moghadam, H.A.; Khavandi, A.; Banaeifar, S. Comparison of Dry Sliding Behavior and Wear Mechanism of Low Metallic and Copper-Free Brake Pads. *Tribol. Int.* **2020**, *151*, 106416. [[CrossRef](#)]
- Chandra Verma, P.; Menapace, L.; Bonfanti, A.; Ciudin, R.; Gialanella, S.; Straffellini, G. Braking Pad-Disc System: Wear Mechanisms and Formation of Wear Fragments. *Wear* **2015**, *322–323*, 251–258. [[CrossRef](#)]
- Xiao, X.; Yin, Y.; Bao, J.; Lu, L.; Feng, X. Review on the Friction and Wear of Brake Materials. *Adv. Mech. Eng.* **2016**, *8*, 1–10. [[CrossRef](#)]
- Yu, D.; Zhou, T.; Zhou, H.; Xu, Y.; Zhang, P.; Yan, Y. Effects of Angle Formation between Melted Zone and Friction Direction on Thermal Fatigue and Wear Resistance of Truck Drum Brake. *Proc. Inst. Mech. Eng. Part D J. Automob. Eng.* **2021**, *235*, 1297–1307. [[CrossRef](#)]
- Li, Z.; Han, J.; Yang, Z.; Li, W. Analyzing the Mechanisms of Thermal Fatigue and Phase Change of Steel Used in Brake Discs. *Eng. Fail. Anal.* **2015**, *57*, 202–218. [[CrossRef](#)]
- Luo, J.; Zhou, X. Superlubricitive engineering—Future industry nearly getting rid of wear and frictional energy consumption. *Friction* **2020**, *8*, 23. [[CrossRef](#)]
- Zhang, P.; Lian, Q.; Deng, G.; Zhu, H.; Li, H.; Wang, X.; Liu, Z. Influence of white etching layer on rolling contact behavior at wheel-rail interface. *Friction* **2020**, *8*, 19. [[CrossRef](#)]
- Zhang, L.; Wei, D.; Wu, P.; Cao, J.; Shijia, C.; Qu, X. A high-performance copper-based brake pad for high-speed railway trains and its surface substance evolution and wear mechanism at high temperature. *Wear* **2020**, *444*, 203182. [[CrossRef](#)]
- Neog, S.P.; Kumar, A.R.; Das Bakshi, S.; Das, S. Understanding the Complexities of Dry Sliding Wear Behaviour of Steels. *Mater. Sci. Technol.* **2021**, *37*, 504–518. [[CrossRef](#)]
- Innocenti, A.; Marini, L.; Meli, E.; Pallini, G.; Rindi, A. Development of a Wear Model for the Analysis of Complex Railway Networks. *Wear* **2014**, *309*, 174–191. [[CrossRef](#)]
- Miab, S.A.; Avishan, B.; Yazdani, S. Wear Resistance of Two Nanostructural Bainitic Steels with Different Amounts of Mn and Ni. *Acta Metall. Sin. (Engl. Lett.)* **2016**, *29*, 587–594. [[CrossRef](#)]
- Moghaddam, P.V.; Hardell, J.; Vuorinen, E.; Prakash, B. Effect of Retained Austenite on Adhesion-Dominated Wear of Nanostructured Carbide-Free Bainitic Steel. *Tribol. Int.* **2020**, *150*, 106348. [[CrossRef](#)]
- Yetim, A.F.; Codur, M.Y.; Yazici, M. Using of Artificial Neural Network for the Prediction of Tribological Properties of Plasma Nitrided 316L Stainless Steel. *Mater. Lett.* **2015**, *158*, 170–173. [[CrossRef](#)]

19. Shah, M.; Das Bakshi, S. Three-Body Abrasive Wear of Carbide-Free Bainite, Martensite and Bainite-Martensite Structure of Similar Hardness. *Wear* **2018**, *402*, 207–215. [[CrossRef](#)]
20. Kasem, H.; Brunel, J.F.; Dufrénoy, P.; Siroux, M.; Desmet, B. Thermal Levels and Subsurface Damage Induced by the Occurrence of Hot Spots during High-Energy Braking. *Wear* **2011**, *270*, 355–364. [[CrossRef](#)]
21. Ammarullah, M.I.; Afif, I.Y.; Maula, M.I.; Winarni, T.I.; Tauviqirrahman, M.; Akbar, I.; Basri, H.; van der Heide, E.; Jamari, J. Tresca Stress Simulation of Metal-on-Metal Total Hip Arthroplasty during Normal Walking Activity. *Materials* **2021**, *14*, 7554. [[CrossRef](#)] [[PubMed](#)]
22. Jamari, J.; Ammarullah, M.I.; Saad, A.P.M.; Syahrom, A.; Uddin, M.; van der Heide, E.; Basri, H. The Effect of Bottom Profile Dimples on the Femoral Head on Wear in Metal-on-Metal Total Hip Arthroplasty. *J. Funct. Biomater.* **2021**, *12*, 38. [[CrossRef](#)] [[PubMed](#)]
23. Xiao, Y.; Zhang, Z.; Yao, P.; Fan, K.; Zhou, H.; Gong, T.; Zhao, L.; Deng, M. Mechanical and Tribological Behaviors of Copper Metal Matrix Composites for Brake Pads Used in High-Speed Trains. *Tribol. Int.* **2018**, *119*, 585–592. [[CrossRef](#)]
24. Vasiljevic, S.; Glišović, J.; Stojanovic, B.; Stojanovic, N.; Grujic, I. The Analysis of the Influential Parameters That Cause Particles Formation during the Braking Process: A Review. *Proc. Inst. Mech. Eng. Part J J. Eng. Tribol.* **2022**, *236*, 31–48. [[CrossRef](#)]
25. Zhang, P.; Zhang, L.; Wei, D.; Wu, P.; Cao, J.; Shijia, C.; Qu, X. Substance Evolution and Wear Mechanism on Friction Contact Area of Brake Disc for High-Speed Railway Trains at High Temperature. *Eng. Fail. Anal.* **2020**, *111*, 104472. [[CrossRef](#)]
26. Lyu, Y.; Bergseth, E.; Wahlström, J.; Olofsson, U. A Pin-on-Disc Study on the Tribology of Cast Iron, Sinter and Composite Railway Brake Blocks at Low Temperatures. *Wear* **2019**, *424*, 48–52. [[CrossRef](#)]
27. Wang, Z.; Han, J.; Domblesky, J.P.; Li, Z.; Fan, X.; Liu, X. Crack Propagation and Microstructural Transformation on the Friction Surface of a High-Speed Railway Brake Disc. *Wear* **2019**, *428*, 45–54. [[CrossRef](#)]
28. Riva, G.; Valota, G.; Perricone, G.; Wahlström, J. An FEA Approach to Simulate Disc Brake Wear and Airborne Particle Emissions. *Tribol. Int.* **2019**, *138*, 90–98. [[CrossRef](#)]
29. Rodrigues, A.C.P.; Österle, W.; Gradt, T.; Azevedo, C.R.F. Impact of Copper Nanoparticles on Tribofilm Formation Determined by Pin-on-Disc Tests with Powder Supply: Addition of Artificial Third Body Consisting of Fe₃O₄, Cu and Graphite. *Tribol. Int.* **2017**, *110*, 103–112. [[CrossRef](#)]
30. Barros, L.Y.; Poletto, J.C.; Neis, P.D.; Ferreira, N.F.; Pereira, C.H.S. Influence of Copper on Automotive Brake Performance. *Wear* **2019**, *426*, 741–749. [[CrossRef](#)]
31. Cai, R.; Zhang, J.; Nie, X.; Tjong, J.; Matthews, D.T.A. Wear Mechanism Evolution on Brake Discs for Reduced Wear and Particulate Emissions. *Wear* **2020**, *452*, 203283. [[CrossRef](#)]
32. Li, W.; Zhang, L.C.; Wu, C.H.; Cui, Z.X.; Niu, C.; Wang, Y. Debris effect on the surface wear and damage evolution of counterpart materials subjected to contact sliding. *Adv. Manuf.* **2022**, *10*, 72–86. [[CrossRef](#)]
33. Jayashree, P.; Federici, M.; Bresciani, L.; Turani, S.; Sicigliano, R.; Straffelini, G. Effect of Steel Counterface on the Dry Sliding Behaviour of a Cu-Based Metal Matrix Composite. *Tribol. Lett.* **2018**, *66*, 123. [[CrossRef](#)]
34. Jayashree, P.; Bortolotti, M.; Turani, S.; Straffelini, G. High-Temperature Tribo-Oxidative Wear of a Cu-Based Metal-Matrix Composite Dry Sliding Against Heat-Treated Steel. *Tribol. Lett.* **2019**, *67*, 110. [[CrossRef](#)]
35. Leonardi, M.; Alemani, M.; Straffelini, G.; Gialanella, S. A Pin-on-Disc Study on the Dry Sliding Behavior of a Cu-Free Friction Material Containing Different Types of Natural Graphite. *Wear* **2020**, *442*, 203157. [[CrossRef](#)]
36. Li, X.; Sosa, M.; Olofsson, U. A Pin-on-Disc Study of the Tribology Characteristics of Sintered versus Standard Steel Gear Materials. *Wear* **2015**, *340*, 31–40. [[CrossRef](#)]
37. Federici, M.; Straffelini, G.; Gialanella, S. Pin-on-Disc Testing of Low-Metallic Friction Material Sliding Against HVOF Coated Cast Iron: Modelling of the Contact Temperature Evolution. *Tribol. Lett.* **2017**, *65*, 121. [[CrossRef](#)]
38. Wu, J.; Ma, B.; Li, H.; Stanciulescu, I. The Running-in Micro-Mechanism and Efficient Work Conditions of Cu-Based Friction Material against 65Mn Steel. *Exp. Tech.* **2019**, *43*, 667–676. [[CrossRef](#)]